JOURNAL OF GEOPHYSICAL RESEARCH, VOL. 108, NO. D5, 8325, doi:10.29/2001JD001034, 2003

# Nonorographic generation of Arctic polar stratospheric clouds during December 1999

Matthew H. Hitchman, Marcus L. Buker, and Gregory J. Tripoli
Department of Atmospheric Sciences, University of Wisconsin, Madison, Wisconsin, USA

Edward V. Browell and William B. Grant
NASA Langley Research Center, Hampton, Virginia, USA

Thomas J. McGee and John F. Burris
NASA Goddard Space Flight Center, Greenbelt, Maryland, USA

Received 6 July 2001; revised 8 February 2002; accepted 8 February 2002; published 10 January 2003.

[1] During December 1999, polar stratospheric clouds (PSCs) were observed in the absence of conditions conducive to generation by topographic gravity waves. The possibility is explored that PSCs can be generated by inertia gravity waves (IGW) radiating from breaking synoptic-scale Rossby waves on the polar front jet. The aerosol features on 7 and 12 December are selected for comparison with theory and with simulations using the University of Wisconsin Nonhydrostatic Modeling System (UWNMS). Consistent with Rossby adjustment theory, a common feature in the UWNMS simulations is radiation of IGW from the tropopause polar front jet, especially from sectors which are evolving rapidly in the Rossby wave breaking process. Packets of gravity wave energy radiate upward and poleward into the cold pool, while individual wave crests propagate poleward and downward, causing mesoscale variations in vertical motion and temperature. On 12 December the eastbound DC-8 lidar observations exhibited a fairly uniform field of six waves in aerosol enhancement in the 14–20 km layer, consistent with vertical displacement by a field of IGW propagating antiparallel to the flow, with characteristic horizontal and vertical wavelengths of ~300 and ~10 km. UWNMS simulations show emanation of a field of IGW upward and southwestward from a northward incursion of the polar front jet. The orientation and evolution of the aerosol features on 7 December are consistent with a single PSC induced by an IGW packet propagating from a breaking Rossby wave over western Russia toward the northeast into the coldest part of the base of the polar vortex, with characteristic period ~9 hours, vertical wavelength ~12 km, and horizontal wavelength ~1000 km. Linear theory shows that for both of these cases, IGW energy propagates upward at ~1 km/hour and horizontally at ~100 km/hour, with characteristic trace speed ~30 m/s. The spatial orientation of the PSC along IGW phase lines is contrasted with the nearly horizontal filamentary structures in the PSC, which are indicative of flow streamlines. It is suggested that vertical displacement is a crucial factor in determining whether a PSC will form and that most PSCs are relatable to specific synoptic and mesoscale motions. *INDEX TERMS:* 0341 Atmospheric Composition and Structure: Middle atmosphere—constituent transport and chemistry (3334); 3362 Meteorology and Atmospheric Dynamics: Stratosphere/troposphere interactions; 3334 Meteorology and Atmospheric Dynamics: Middle atmosphere dynamics (0341, 0342); 3349 Meteorology and Atmospheric Dynamics: Polar meteorology; 3329 Meteorology and Atmospheric Dynamics: Mesoscale meteorology; *KEYWORDS:* gravity waves, polar stratospheric clouds (PSCs), synoptic waves, mesoscale modeling, Rossby wave breaking, ozone

**Citation:** Hitchman, M. H., M. L. Buker, G. J. Tripoli, E. V. Browell, W. B. Grant, C. Hostetler, T. J. McGee, and J. F. Burris, Nonorographic generation of Arctic polar stratospheric clouds during December 1999, *J. Geophys. Res.*, *108*(D5), 8325, doi:10.1029/2001JD001034, 2003.

## 1. Introduction

[2] A primary purpose of the SAGE III Ozone Loss and Validation Experiment (SOLVE) during December 1999 to March 2000 was to investigate the role of polar stratospheric clouds (PSCs) in Arctic ozone depletion. From

Copyright 2003 by the American Geophysical Union.
0148-0227/03/2001JD001034$09.00

previous work on Arctic PSCs it was expected that flow over topography, such as the Scandinavian shield, would generate gravity waves which disturb the lower stratosphere, leading to particle condensation, hence conversion of ozone-destroying chemical species to active form [e.g., *Cariolle et al.*, 1989; *Volkert and Intes*, 1992; *Leutbecher and Volkert*, 1996; *Meilinger et al.*, 1995; *Whiteway and Duck*, 1996; *Carslaw et al.*, 1998a, 1998b; *Dörnbrack et al.*, 1998; *Wirth et al.*, 1999]. Many PSCs associated with orography were observed during January and March, but during December the observed PSCs were not generally found near orographic features. While carrying out forecasts for each flight using the University of Wisconsin Nonhydrostatic Modeling System (UWNMS) in Kiruna, Sweden, it was realized that a typical feature of the model is radiation of inertia gravity waves (IGW) from adjusting larger-scale flows.

[3] *O'Sullivan and Dunkerton* [1995] employed a sector model of baroclinic life cycles and found that IGW are preferentially radiated upward and poleward from the warm upglide sector of a breaking synoptic Rossby wave. Recent observational studies of gravity waves in the polar stratosphere [e.g., *Whiteway et al.*, 1997; *Yoshiki and Sato*, 2000; *Pfenninger et al.*, 1999] conclude that a substantial fraction of IGW are generated by flow adjustment processes associated with tropospheric weather systems or the stratospheric polar night jet. *Yoshiki and Sato* [2000] employed high-resolution radiosondes and showed that near selected Arctic stations most of the wave energy propagates upward. They found that over Antarctic stations some of the wave energy propagates downward from the polar night jet. *Sato et al.* [1999] used a high-resolution aqua planet model and found a broad spectrum of IGW associated with polar flow adjustment. Here we employ lidar observations for 7 and 12 December 1999 and UWNMS simulations to explore the hypothesis that this type of mesoscale motion can disturb the cold pool and generate PSCs.

[4] The lidar temperature, ozone, and aerosol measurement techniques are described in section 2, along with aspects of the UWNMS simulations. An overview of the December SOLVE PSCs is given in section 3. In section 4 the lidar aerosol enhancements seen on 12 December are shown first, as an example of a horizontally extensive, uniform wave pattern. This is compared with UWNMS simulations, which show IGW of comparable scale and slope radiating back along the outbound flight from a distinctive northward polar front jet south of Severnaya Zemlya. In section 5 the PSC lidar observations and UWNMS results for 7 December 1999 are shown, where a large PSC occured in the cold pool, which is disturbed by IGW emanating from a break on the polar front jet over western Russia. Section 6 briefly considers linear gravity wave theory, IGW emission from breaking Rossby waves, draws a distinction between flow streamlines and the macroscopic shape of the PSC, and comments on meteorological factors relevant to PSC formation.

## 2. Observations and UWNMS Specifications

### 2.1. Observations

[5] Lidar time-height sections of temperature, aerosol, and ozone above the DC-8 flight track are particularly useful for constraining the possible dynamical motions responsible for PSCs. Temperature profiles from the Airborne Raman Ozone, Temperature, and Aerosol Lidar (AROTEL) [*Gross et al.*, 1997; *Burris et al.*, 1998] are used here to help characterize the thermal environment of the aerosol features. AROTEL temperature profiles will be compared with a radiosonde profile at Ny Ålesund, Goddard Space Flight Center Data Assimilation Office (GSFC DAO) global data, and with UWNMS temperatures initialized from global meteorological data sets.

[6] The Langley UV DIAL lidar system has provided reliable, high-resolution observations for a variety of DC-8 research campaigns [*Browell et al.*, 1998; *Grant et al.*, 1998]. Differential absorption between 300 and 310 nm enables ozone detection. Here the ratio of observed backscatter at 1064 nm to that expected from Rayleigh scattering by molecules is used to illustrate aerosol features. For SOLVE the vertical averaging interval was 750 m for ozone and 150 m for aerosol, with a vertical display interval of 75 m. With a DC-8 cruising speed of 233 m/s (~14 km/min or 840 km/hour), 30 second temporal averaging yields a horizontal resolution of 7 km for aerosol. For ozone below 19 km altitude, 5 min averaging implies a horizontal resolution of 70 km, while above 19 km 10 min averaging implies a resolution of 140 km. Ozone data are truncated when the standard error exceeds 10% of the average, usually near 25 km altitude. Measurement accuracy is better than 2–3% for aerosol parameters and better than 10% for ozone.

[7] A NOAA-14 satellite image for 7 December 1999 is useful in delineating synoptic features. The channel 5 infrared signal converted to color-enhanced brightness temperature highlights the coldest upper tropospheric clouds in dark gray.

### 2.2. UWNMS Specifications

[8] The UWNMS was initially designed to study tropospheric-scale interaction problems and has been applied to tropical cloud clusters, hurricanes, midlatitude cyclones, polar lows, gravity waves, lake effect snow storms, and mesoscale convective complexes [*Tripoli*, 1992a, 1992b; *Pokrandt et al.*, 1996; *Buker*, 1997; *Jascourt*, 1997; *Mecikalski and Tripoli*, 1997; *Avissar et al.*, 1998]. It includes multiple interactive grid nesting, tropospheric microphysics, radiative transfer, surface processes, and 1/6° (~18.5 km) resolution topography. Operational tropospheric weather forecasts are available daily on the internet at http://mocha.aos.wisc.edu. The UWNMS has been adapted for application to transport problems involving the troposphere and lower stratosphere, including a study of ozone transport by synoptic waves out of the Arctic summer stratosphere [*Hitchman et al.*, 1999].

[9] The UWNMS simulations for SOLVE were carried out in the field under the constraint that a complete simulation for the flight day had to be ready at least 24 hours in advance. This required starting the model two days in advance. The model was initialized with National Center for Environmental Prediction aviation model forecasts (NCEP AVN). The horizontal boundaries of the UWNMS were updated every time step from a temporal and spatial interpolation of the 6-hourly 1.0° AVN forecast files. Vertical resolution varied from 300 to 400 m, and the model

top was near 30 km. An 8-point Rayleigh friction sponge layer near the top of the domain and a 5-point Rayleigh friction zone at the horizontal boundaries were implemented to suppress spurious wave reflection. Model variables were archived every 5 min for diagnosis using VIS-5D [*Hibbard and Santek*, 1989].

[10] The 12 December flight revealed a sequence of aerosol thickenings while traveling outbound toward the east and north. The UWNMS forecast in the field was carried out at 55 km horizontal resolution over a 120 × 120 grid domain centered at 70°N, 57°E. It was initialized with the 24 hour AVN forecast and integrated with a 60 s time step from 1200 UT, 11 December to 0000 UT, 13 December 1999. The forecast simulation showed IGW radiating from different active regions of the polar front jet. For post-analysis we re-ran this simulation at 25 km resolution centered at 77°N, 77°E, integrated from 0000 UT, 12 December to 0000 UT, 13 December 1999, with a 30 s time step. At the higher resolution, waves of a scale similar to the aerosol thickenings were found emanating from an isolated northward jet to the east of Severnaya Zemlya. Results from this higher resolution simulation will be discussed in section 4.

[11] A simulation of the environment of the PSC on 7 December will be described in section 5. The UWNMS was integrated from 1200 UT, 6 December to 0000 UT, 8 December 1999, with a 60 s time step and horizontal and vertical resolutions of 55 km and 300–400 m. A horizontal grid of 100 × 100 points was chosen, centered at 75°N, 57°E, with 75 vertical levels extending from 0 to 30 km.

[12] An ''anomaly'' value is defined to be the local departure from the horizontal model domain average of that variable. Ertel's potential vorticity (PV) was calculated using centered differences. PV normalized by $10^6$ $m^2$ K $kg^{-1}$ $s^{-1}$ (here referred to as 1 PVU) will be shown.

## 3. December 1999 SOLVE Campaign

[13] The UWNMS was employed to make forecasts at Arena Arctica, in Kiruna, Sweden, for each of the DC-8 flights on 5, 7, 10, and 12 December. Discussion with the science team provided useful flexibility in choosing the model domain and calling our attention to potential features of interest. Sometimes changes in the flight plan could be supported by running another simulation. During the December campaign weak tropospheric winds were not very favorable for generating orographic gravity waves, yet our simulations showed mesoscale vertical motions in the cold pool which could be related to PSC formation. A common feature of the model was radiation of IGW from evolving jet structures. Since this is to be expected from theory and from tropospheric observational and modeling studies, we began to focus on this mechanism during the campaign.

[14] The PSCs found during December include one near Spitzbergen on the 5th, one on the 7th over the Laptev Sea near Severnaya Zemlya and one near Franz Joseph Land on the 10th. On the 12th a small PSC was found over the Laptev Sea, and there were 6 sinusoidal ''thickenings'' of aerosol in the 15–20 km layer on the outbound flight.

[15] Since many microphysical processes have temperature thresholds, it is important to gauge the fidelity of the UNWMS temperature structures. Figure 1 shows a comparison of the AROTEL lidar and Ny Ålesund radiosonde temperature profiles over Spitzbergen on 2 December 1999. In the 22–27 km layer temperatures were in the range 193–195 K. The tropopause near 9 km (not shown) was topped by an isothermal layer immediately above. The DC-8 flew within a few km of Ny Ålesund, about 1.5 hours after the radiosonde launch. Differences in structure at smaller scales can occur from the time separation. Since the two profiles agree to within ~3 K, AROTEL curtain temperature profiles provide useful guidance for assessing UWNMS temperatures. AROTEL lidar temperature observations and DAO analyses are used to compare with UWNMS modeled temperatures in section 5.

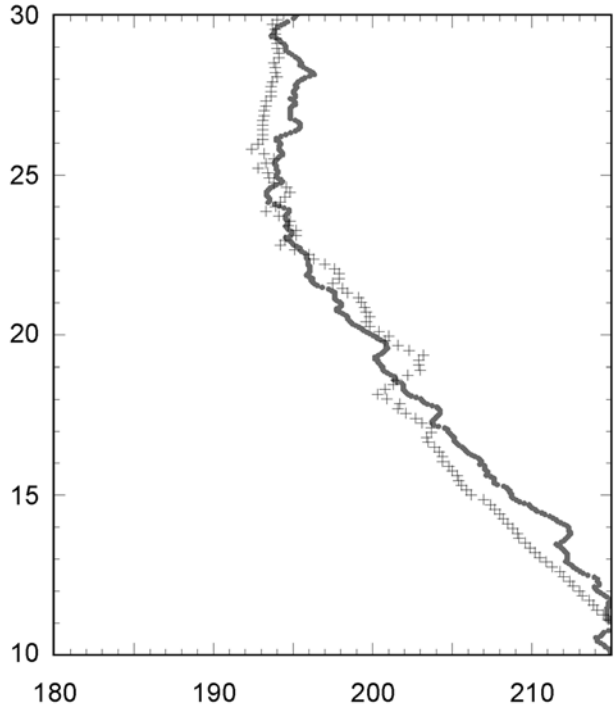


**Figure 1.** Comparison of temperature profiles over Ny Ålesund, Spitzbergen on 2 December 1999 (angle symbols for AROTEL lidar at 1023 UT, thick line for radiosonde at 1210 UT).

## 4. DC-8 Flight of 12 December 1999

[16] On this date a spatially extensive wave pattern in aerosol scattering ratio was observed above the outbound flight. Figures 2 and 3 show the flight track for 12 December and the 1064 nm aerosol scattering ratio for a portion of the flight. Numbers indicate locations of enhanced aerosol scattering ratio. During ~1140–1340 UT the DC-8 was traveling northeastward or eastward (Figure 2), during which six aerosol enhancement regions were encountered in the 15–20 km layer (Figure 3). At the far eastern turn near 1430 UT a small PSC (feature 7 on Figure 2) was observed at 19 km over the Laptev Sea (not shown). The aerosol enhancement features are regularly spaced and tilt downward toward the north and east. Assuming that organized, regularly spaced vertical motion patterns are associated with these features, they could be

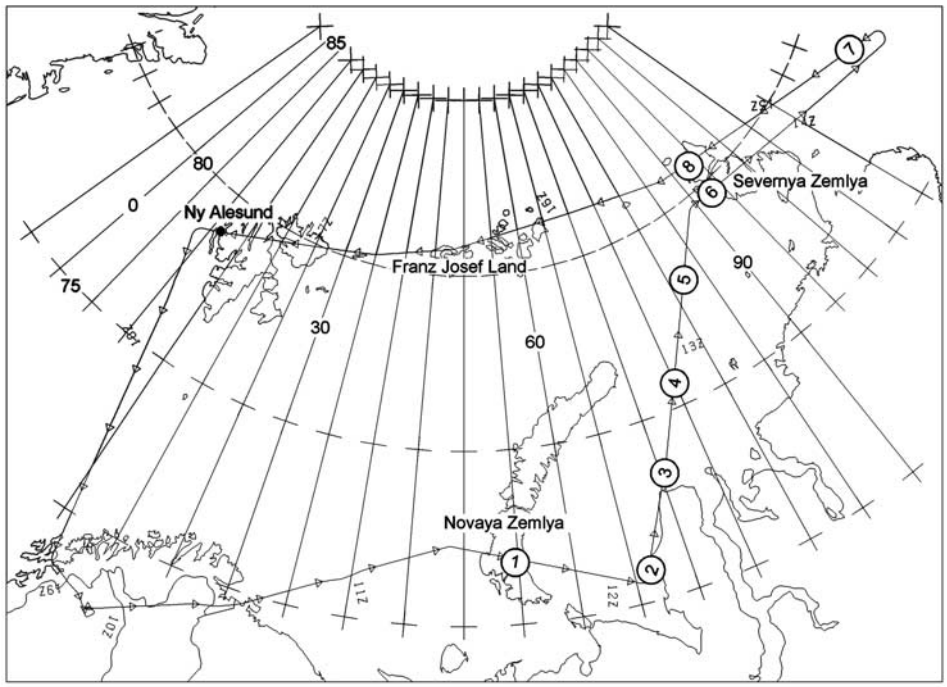


**Figure 2.** Plan view of DC-8 flight during 0950–1923 UT on 12 December 1999. Triangles are spaced 15 min apart and indicate flight direction. Circled numbers indicate a sequence of aerosol enhancement features.

caused by a nearly uniform field of southeastward propagating gravity waves extending about 1500 km along the edge and into the cold pool. As will be shown, surface winds were light to moderate over modest topography, but a distinctive northward jet is present at the tropopause near the eastern edge of the flight track.

[17] Between 1140 and 1340 UT the DC-8 passed through 5 wavelengths. Since the DC-8 traveled ~1680 km during these two hours, this suggests a horizontal wavelength of ~300 km along a straightened flight path. If the IGW crests are intersecting the flight track at an angle, this would be an upper bound on the horizontal wavelength.

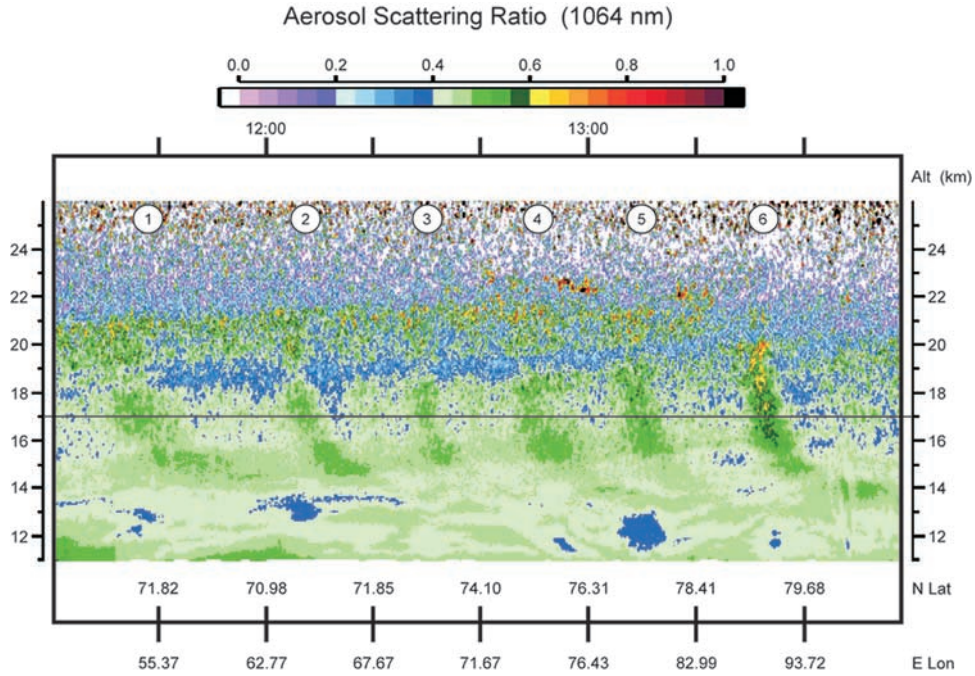


**Figure 3.** Time-altitude section of Langley UV DIAL 1064 nm aerosol scattering ratio during 1120–1400 UT on 12 December 1999. Circled numbers correspond to locations in Figure 2.

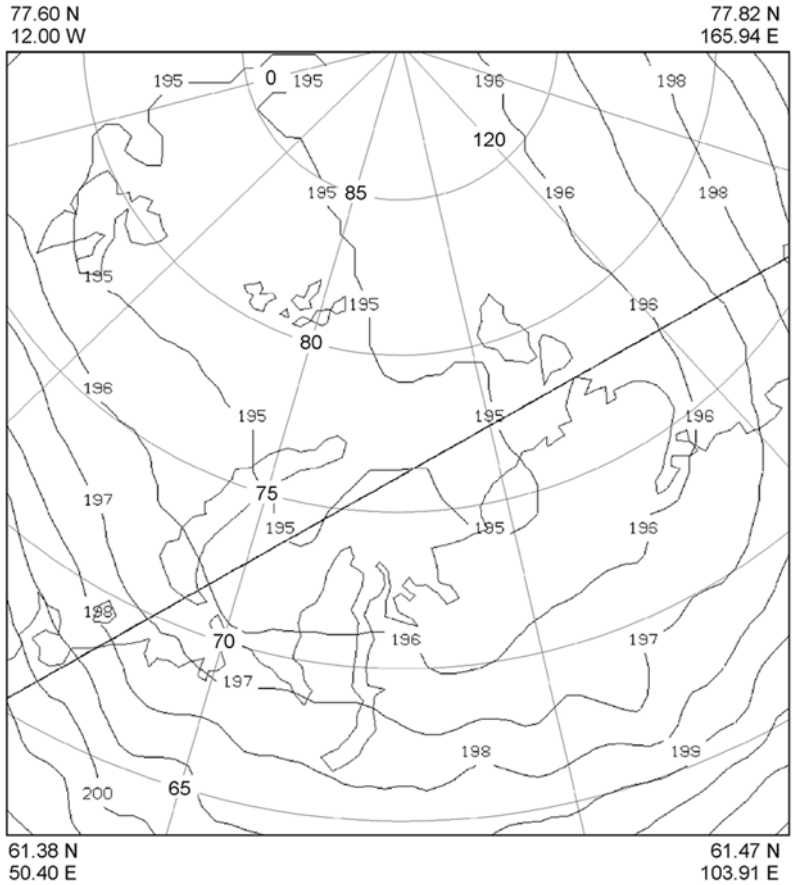


**Figure 4.** UWNMS 20 km temperature forecast for 1240 UT on 12 December 1999 contour interval 1 K. The line shows the location of the cross section in Figure 5, roughly oriented along the flight track in Figure 2.

It will be argued that, since winds near 16 km were nearly parallel to the DC-8 path, gravity waves which survived to that level were likely traveling antiparallel to the aircraft [e.g., *Dunkerton and Butchart*, 1986]. Assuming that the DC-8 was traveling opposite to the IGW phase velocity, an apparent shortening of the wavelength by ~10% would occur. 300 km is taken as a reasonable estimate of horizontal wavelength for these observed aerosol features.

[18] By extrapolating from their tilt in the 16–20 km layer, one may estimate a vertical wavelength of ~10 km. The vertical wavelength increases upward, as may be expected from dispersion from a discrete source. Energy associated with shorter vertical scales travels along a shallower trajectory and is manifested at lower levels, while energy associated with taller gravity waves travels along a steeper trajectory and so is seen preferentially at upper levels [e.g., *Coy and Hitchman*, 1985]. This effect is more pronounced in shear, as upward wave activity traveling downshear gets absorbed, while waves traveling upshear appear taller [*Coy and Hitchman*, 1985].

[19] Figure 4 shows UWNMS temperatures at 20 km, 1240 UT, 12 December. A southeastward elongation of the cold pool is seen between Novaya Zemlya and Severnaya Zemlya, with values above 194 K. Temperatures gradually increase downward (cf. Figure 1), so robust PSCs would not be expected in the 14–20 km layer. Yet vertical displacement and cooling can alter the amount of material in vapor and condensed phases.

[20] The line in Figure 4 shows the orientation of the section shown in Figure 5, roughly parallel to the flight track. The eastward wind shear is parallel to these temperature contours. Contoured UWNMS meridional winds at 1240 UT, 12 December show the polar vortex above 15 km sweeping southward then northward from left to right across the section (Figure 5). In the upper troposphere a northward meridional jet with peak speed exceeding 25 m/s is located just to the east of Severnaya Zemlya, flanked by two regions of southward flow of −5 to −10 m/s (Figure 5). The shaded vertical motion field shows a uniform field of gravity waves extending upward and southwestward from the sharp northward jet at the tropopause. The predominant orientation of the wave field above ~12 km is tilted upward and to the left in this section. In a VIS5D film a wave packet is emanated as the jet penetrates poleward (not shown). These modeled waves have a vertical wavelength of 5–10 km and a horizontal wavelength of ~300 km.

[21] The waves represented in the UWNMS are sensitive to model grid spacing, initial conditions, and other aspects. This implies inherent uncertainty in size, location, and timing of events. We interpret the UWNMS results as illustrative of

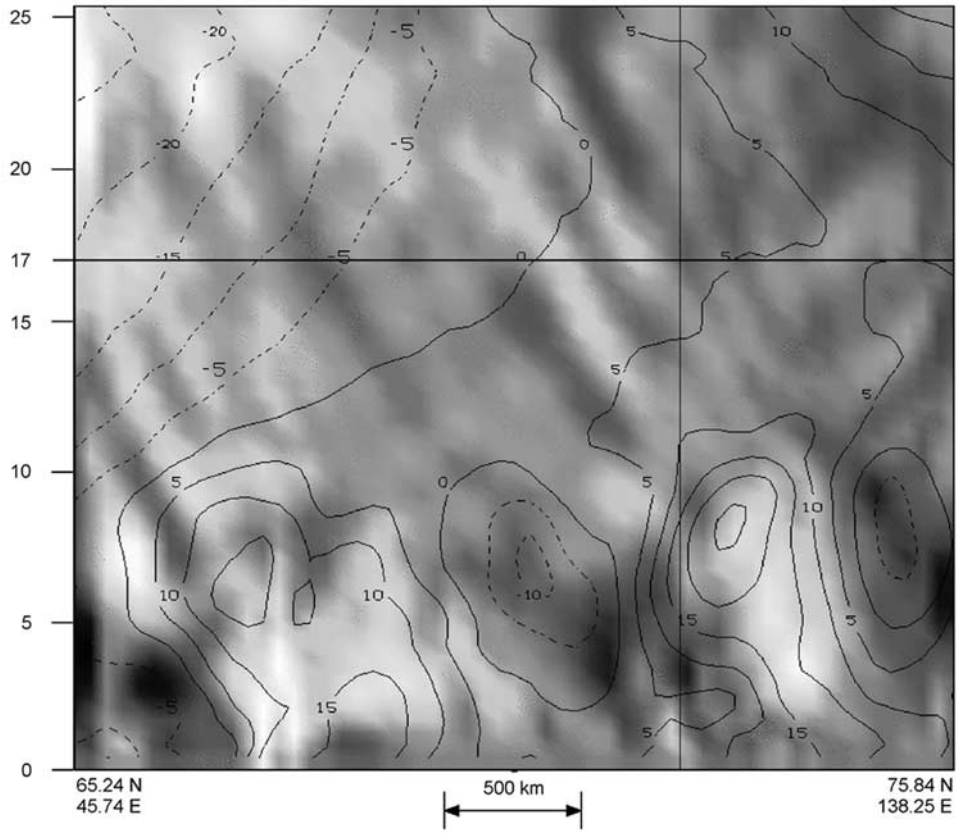


**Figure 5.** Cross section of UWNMS meridional wind (contours every 5 m/s) and vertical wind (dark downward, light upward) along the line in Figure 4 at 1240 UT, 12 December 1999.

the mechanism, lending insight into the likely location of the disturbance which generated the aerosol thickenings: to the east of the flight track near the tropopause.

[22] Figure 6 shows UWNMS horizontal wind vectors and speed contours at 1, 9, and 16 km at 1240 UT, 12 December 1999. A surface low west of Novaya Zemlya is related to a surge of air from the south toward Novaya Zemlya (Figure 6a). A second region of broad northward flow is found east of Severnaya Zemlya. Figure 6b shows a distinctive tropopausal meridional jet, extending from Siberia into the Laptev Sea just east of Severnaya Zemlya. Following the terminology of *Palmén and Newton* [1969], we refer to this as a northward excursion of the "polar front jet". At 16 km the flow is uniformly under the influence of the polar vortex (Figure 6c). At this level it can be seen that the flow is roughly parallel to the outbound DC-8 path. It will be argued in section 6 that the winds should filter gravity waves emanating from the meridional tropopause jet such that the expected waves will have crests oriented upward, southwestward above the outbound DC-8.

## 5. Flight of 7 December 1999

[23] The DC-8 flight path on 7 December is shown in Figure 7. Segments of the flight where the Langley UV DIAL system detected PSC particles are highlighted: between 1225 and 1340 UT spanning the turn over the Laptev Sea, and between 1430 and 1455 UT northbound just west of Severnaya Zemlya. AROTEL temperatures along the flight path (color, Figure 8) suggest that during 1230–1500 UT the DC-8 flew under temperatures less than 192 K in the 20–25 km layer. A small patch of ~186 K is seen near 1230 UT, 22 km in the AROTEL data. This cold pattern extends downward with time to about 1330 UT, 18 km. The cold pool seen in the DAO analysis (thin solid contours) is centered a km or two higher and is not quite as cold as shown by AROTEL. Since the aerosol features coincided with minimum AROTEL temperatures, it is likely that AROTEL temperatures represent a realistic local cold feature.

[24] The UWNMS 22 km temperature forecast at 1200 UT, 7 December, is shown in Figure 9. At this level part of the cold pool was centered between Novaya Zemlya and Severnaya Zemlya, with an area less than 192 K. Figure 8 shows that near this level AROTEL temperatures are slightly cooler, while DAO temperatures are slightly warmer than UWNMS temperatures. The strength of the horizontal temperature gradient in Figure 9 indicates where winds are increasing upward into the polar night jet. The temperature field shows wavy disturbances ranging from ~3 K in the strong jet to the south, to ~0.5 K approaching the cold pool. These arise in the model via radiation of inertia gravity waves from the tropopausal polar front jet.

[25] A portion of the UV DIAL aerosol and ozone observations for 7 December are shown in Figures 10 and 11. The outline of the two aerosol features are transposed onto the ozone section. Two 120° right-hand turns were executed near

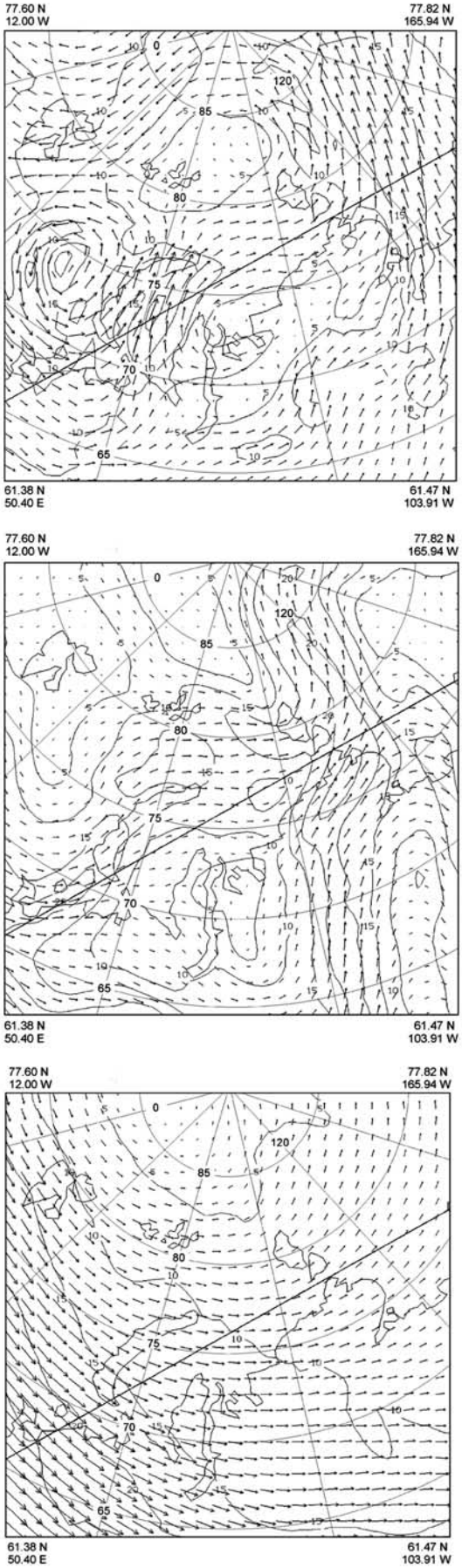


1300 and 1400 UT (Figure 7). The first observed feature, "PSC1", was encountered at 1225 UT, ~200–300 km north of Severnaya Zemlya (cf. Figure 7). Its western edge was over 2 km thick, extending from 21 to 23 km. Over the subsequent 80 min, which included a turn, "PSC1" was observed to tilt downward and to diminish in thickness. Accounting for the flight geometry, "PSC1" was at least 400 km across and probably larger. Along the 100°E meridian, the aspect ratio was ~1:100. Near the tip of "PSC1" (18 km, 1340 UT) an axis of low ozone extended down to 16 km near 1400 UT (Figure 11).

[26] "PSC2" was encountered during 1430–1455 UT and was at least 350 km in length. "PSC2" tilted northward along the flight track, was about 2 km thick, and extended from 18.5 km at its southern end to 23 km at the poleward end. Its aspect ratio in this plane was ~1:80. Near the southern tip of "PSC2" (19 km, 1430 UT) a very similar axis of low ozone extended down to 16 km near 1420 UT. Note also the concave downward shape of the ozone maximum near 21 km. This distinctive ozone structure depicts the center of the bottom of the polar vortex.

[27] The DC-8 was located near 82.5°N, 90°E at 1210 and 1450 UT (Figure 7). "PSC1" was first encountered about 10 min (~140 km) after the track crossing point, while "PSC2" was present at the crossing point 2 hours and 40 min later. Due to the difference in slope and lack of spatial and temporal coincidence one might conclude that these two observational events are distinct PSCs. Alternatively, one may view this as one PSC which tilted strongly downward toward the south and moderately toward the east, and that it propagated and developed during this period. This would require its northwestern edge to develop westward at least 120 km in less than 3 hours (~13 m/s). Horizontal winds in the 19–24 km layer over Severnaya Zemlya in the UWNMS were ~2 m/s from the northeast. A dynamically static phenomenon could be advected westward only about 15 km during this time, not enough to close the gap. IGW, however, can readily propagate this distance in a few hours, inducing upward motion and particle condensation. These observations and simulations to be shown are compatible with the view that this is a single, evolving PSC.

[28] Further observational evidence regarding the dynamical origin and nature of the flow through the PSC is found in Figure 12, which highlights infrared scattering ratios exceeding 0.1 in black. At least 8 filaments are observed across the ~4500 m depth of the PSC. These filaments are each only a few hundred meters thick, but are well resolved at 75 m. This suggests that differential horizontal advection in the cold pool upstream of the PSC juxtaposed air with differing amounts of condensible material in the vertical. Since these filaments are nearly material surfaces, they can be taken as good indicators of the wind streamline pattern through the PSC. While streamlines tend to tilt upward toward the north, this is clearly less steep than the tilt of the PSC as a whole. It will be shown that these features are compatible with generation by an IGW.

**Figure 6.** (opposite) Plan view of UWNMS wind vectors and wind speed (contours every 5 m/s) at (a) 1 km, (b) 9 km, and (c) 16 km at 1240 UT on 12 December 1999.

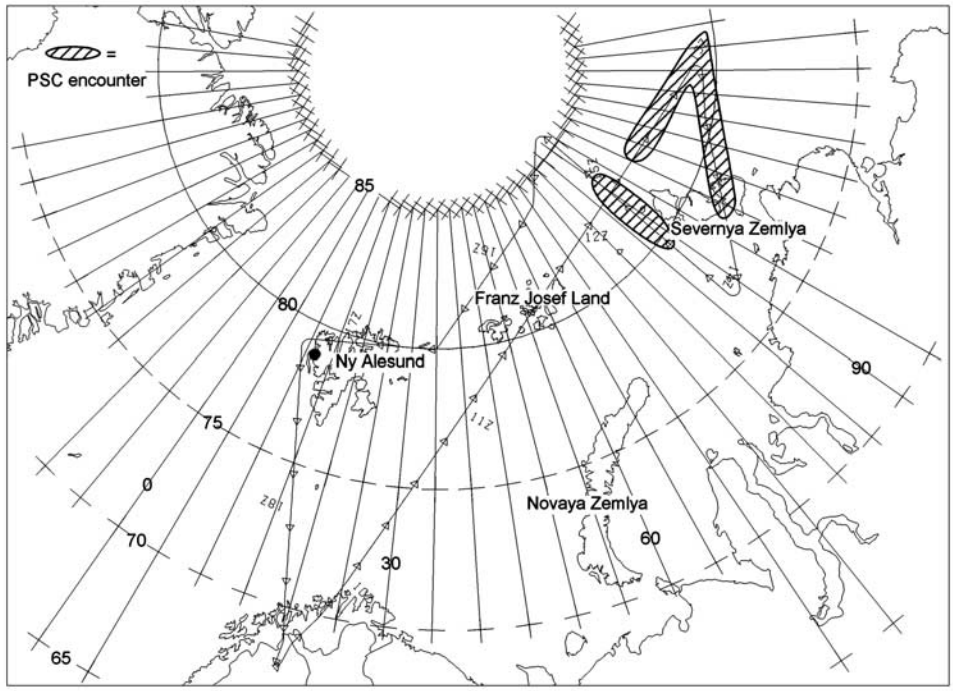


**Figure 7.** Plan view of DC-8 flight during 0920–1858 UT on 7 December 1999. Triangles are spaced 15 min apart and indicate flight direction. "PSC1" was found near the easternmost turn (1220–1340 UT), while "PSC2" was found just northwest of Severnaya Zemlya (1430–1455 UT).

[29] Tropospheric cloud features and UWNMS wind forecasts are shown in Figures 13 and 14. In the infrared satellite image at 1119 UT one may see the northern portion of Scandinavia and the location of Kiruna at lower left. East of Finland the pattern in upper tropospheric cirrus indicates the presence of a developing synoptic disturbance, with a warm upglide sector near 40–60°E, 65°N. The end of the counterclockwise cloud spiral is located above the surface low, as seen in the UWNMS 1 km wind pattern at 1300 UT (Figure 14a). Note the weak anticyclone in the lower troposphere just to the east of Severnaya Zemlya (Figure 14a). Near the tropopause at ~60°N, 45°E (Figure 14b) a

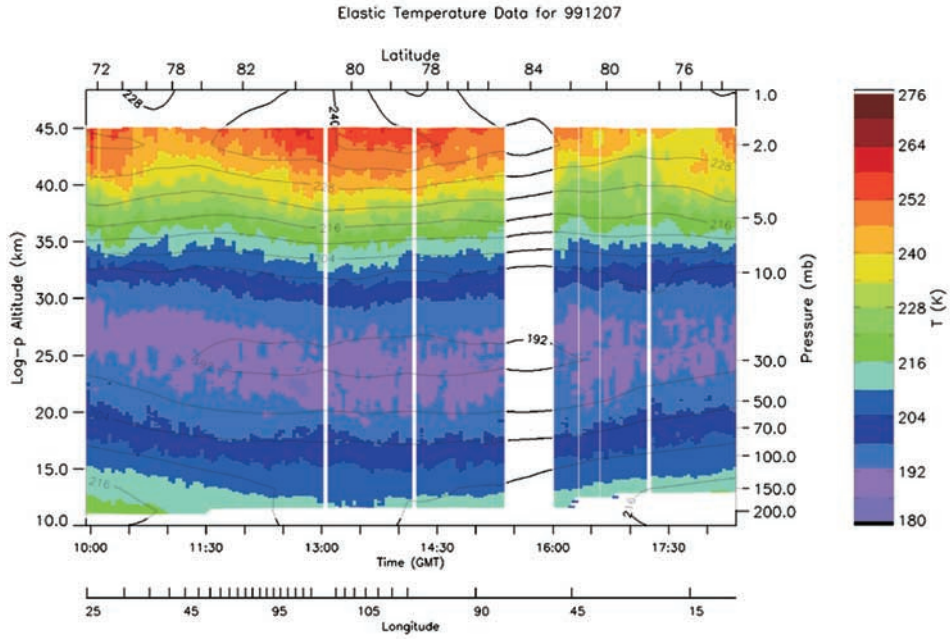


**Figure 8.** Time-height section of AROTEL lidar temperature (color) above the DC-8 for the flight of 7 December 1999. Note temperatures less than 192 K in the 22–25 km layer from 1300 to 1500 UT. Temperatures from the GSFC DAO analysis are also shown, contour interval 6 K.

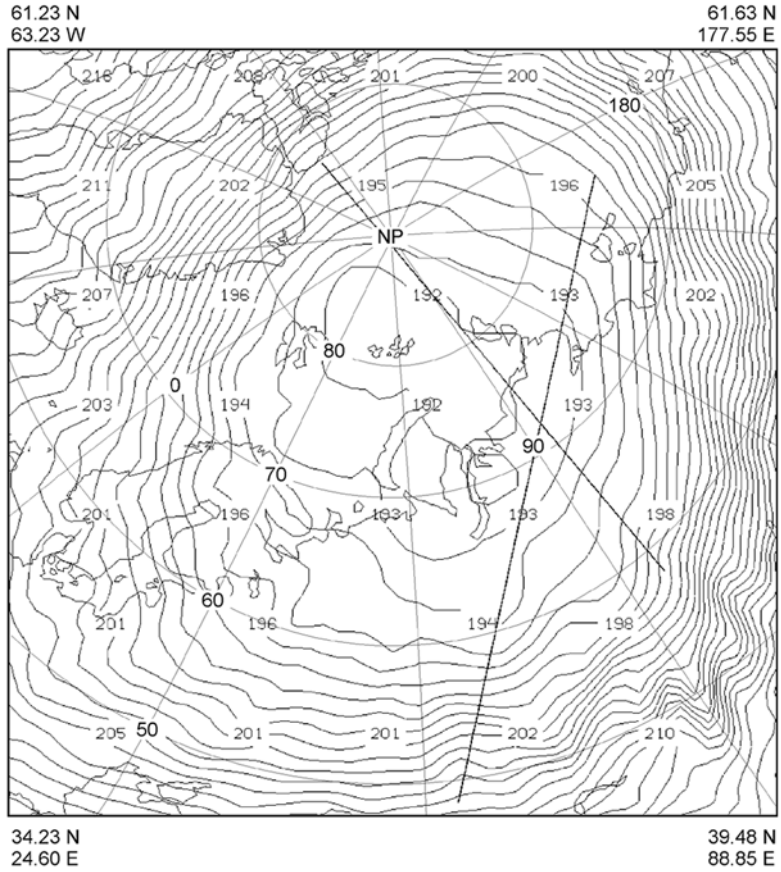


**Figure 9.** UWNMS 22 km temperature forecast for 1300 UT on 7 December 1999, contour interval 0.5 K. The southwest-northeast line shows the location of the sections in Figure 15. The north-south line is tangent to the flight path where "PSC2" was found and shows the location of the section in Figure 16.

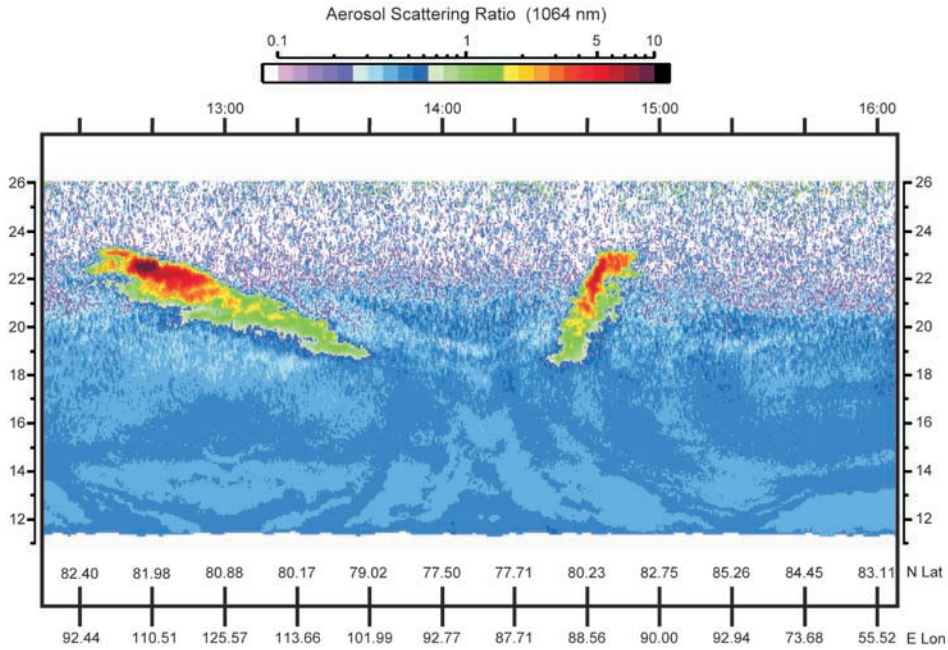


**Figure 10.** Time-altitude section of LaRC lidar 1064 nm aerosol scattering ratio during 1200–1600 UT on 7 December 1999. "PSC1" was underflown during 1220–1340 UT, then "PSC2" during 1430–1455 UT. The boundaries of these aerosol features were transcribed onto the ozone section in Figure 11.

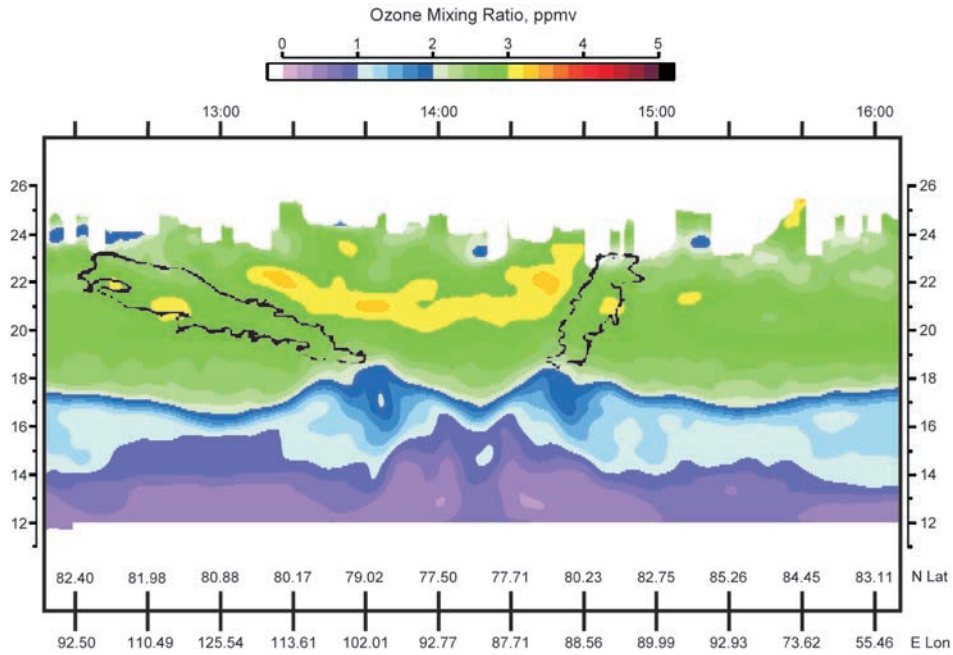


**Figure 11.** Same as Figure 10, except of the ozone mixing ratio (ppmv). The boundaries of the aerosol features in Figure 10 are shown.

region of low PV air extends northeastward, while to the east, high PV air extends to the south and west in a classical Rossby wave breaking pattern. The center of the polar vortex at 20 km was located very close to the corner of the flight track near 1400 UT (Figures 7 and 14c).

[30] An intriguing cirrus cloud was seen north of Severnaya Zemlya (Figure 13). It was oriented northeast-southwest, exceeded 100 km in length, and was likely in the 8–10 km altitude range. It supports the concept that it was quite cold near the tropopause, below the base of the polar vortex. Although this cirrus cloud near 9 km is much smaller and of a different shape than the PSC near 20 km, its proximity to Severnaya Zemlya raises the possibility of orographic gravity waves. Surface winds near Severnaya Zemlya were from the south at 5 m/s or less (Figure 14a). At 20 km (Figure 14c) the flow near the north end of Severnaya Zemlya was less than 2 m/s and from the northeast. These conditions are not favorable for the excitation or vertical transmission of orographic (quasistationary) gravity waves.

[31] Two cross sections of UWNMS zonal wind (contours) and vertical motion (shaded) at 1030 and 1300 UT, 7 December are shown in Figure 15. The northeastward orientation of this section (illustrated as a straight line on Figure 14) was chosen after detailed inspection of the VIS5D movie (not shown), in which a packet of gravity waves emanated from the strong fold in the polar front jet over western Russia (Figure 14b). This section grazes the southern edge of the cold pool and so has warmer temperatures, but it is most representative of the wave field that influenced the stratosphere over Severnaya Zemlya. Temperatures are contoured at and below 198 K (white lines). Cross-hairs indicate the location of the PSC a little to the north of the section. The polar front jet over western Russia is seen at the lower left, reaching 60 m/s. In Figure 15 three distinct crests of upward motion extend poleward and upward from the break in the polar front jet. The vertical wavelength is ~12 km, and the horizontal distance between wave crests is ~1000 km. For the IGW in Figure 15,

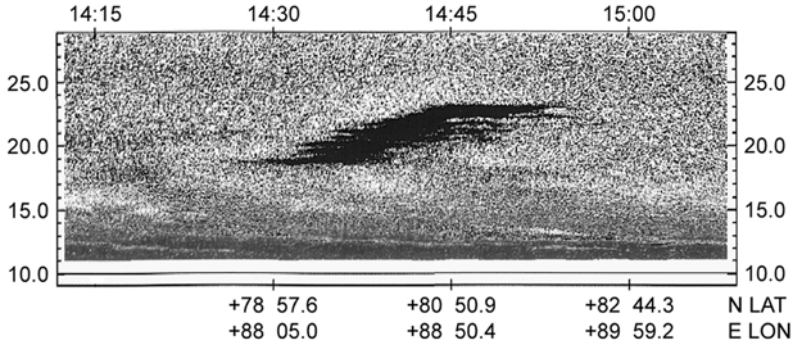


**Figure 12.** Time-altitude section of 1064 nm aerosol scattering ratio for "PSC2" on 7 December 1999, with values exceeding 0.1 emphasized in black.

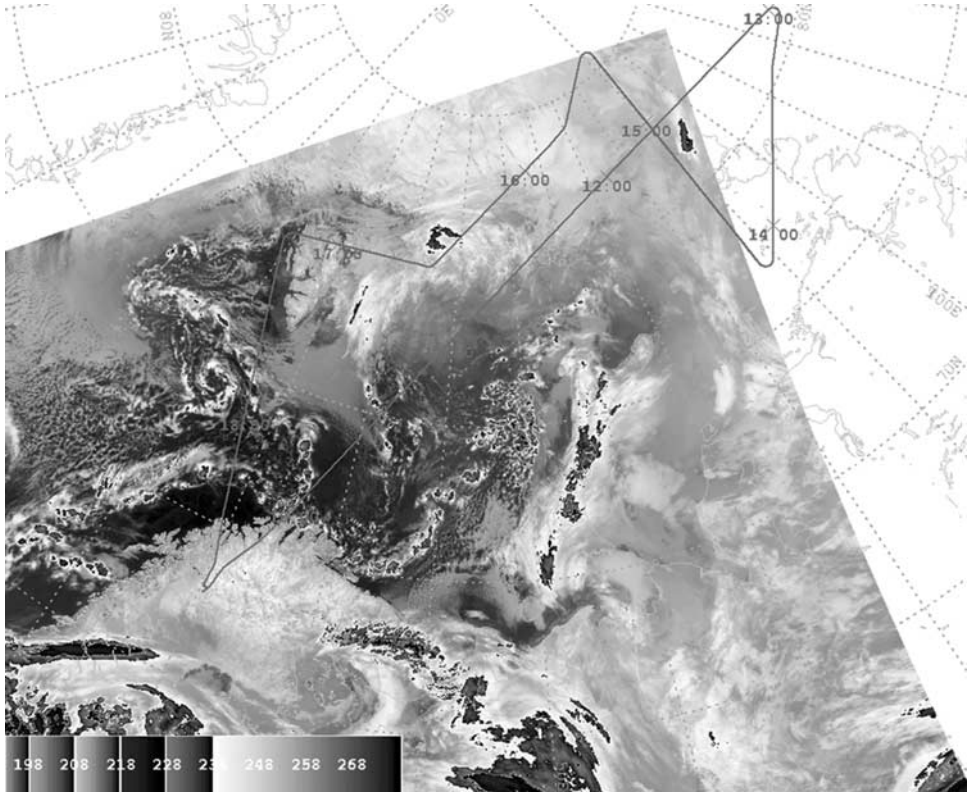


**Figure 13.** Enhanced infrared image of the European Arctic from NOAA channel 5 at 1119 UT on 7 December 1999, with flight track superimposed. Note the cirrus cloud near the northern tip of Severnaya Zemlya and the tropopause synoptic wave east of Finland.

horizontal and vertical variations are equally resolved in the model (about 20 model grid points per wavelength). The region of upwelling motion to the left of the crosshairs reaches a maximum of ~1 cm/s, and propagates down and to the right ~1/6 wavelength during the 1.5 hour interval between Figures 15a and 15b.

[32] A VIS5D movie (not shown) clearly reveals Rossby wave breaking on the morning of 7 December and emanation of gravity wave activity poleward and upward from the tropopause. Consistent with gravity wave theory, as the energy traveled poleward and upward, individual wave crests formed on the leading edge and propagated downward into the cold pool. These waves had propagation speeds on the order of 30 m/s, similar to the jet from which they emanated, and had periods on the order of 6–8 hours. These simulations suggest that during 1100–1400 UT the region near the PSC experienced IGW motions originating near the tropopause to the south and west.

[33] Figure 16 shows a snapshot of UWNMS vertical motion and stream function in a section tangent to the northbound flight track near Severnaya Zemlya (Figures 7 and 14). Note the descent and divergence in the lower tropospheric anticyclone (Figure 14a). The location of "PSC2" at 1400 UT is shown as bold cross-hairs. At 1100 UT in the model there is a coherent region of upward motion in the 18–24 km layer, tilting poleward with altitude, similar in orientation and tilt to "PSC2" (compare Figures 12 and 16). Due to the transient nature of these propagating waves, actual particle motions were more horizontal than this snapshot of meridional stream function would suggest.

[34] Particle trajectories were calculated using VIS5D. Particles were selected which intersected the bottom, middle and top of "PSC1" and "PSC2" when observed by the DC-8. Horizontal air flow in the cold pool was nearly stationary. The ~2 m/s northeasterly flow at these levels would cause a horizontal drift of ~200 km during the 28 hour integration. As IGW passed through the cold pool, particles experienced vertical motions. During ~1000–1300 UT upward motion of order 5 mm/s occurred, suggesting a vertical displacement of ~50 m over a 3 hour period. From the linearized eddy temperature equation, $T' \sim -\overline{T}N^2\,\delta z/g$, this would correspond to a temperature perturbation of ~0.4 K. These small vertical excursions are compatible with the nearly horizontal orientation of the filaments in Figure 12 relative to the tilt of the PSC.

## 6. Discussion and Conclusions

[35] Linear gravity wave theory provides a useful framework for interpreting these observations and model results. This theory is consistent with the idea that many of the aerosol features in December 1999 were caused by IGW radiating from the polar front jet. It allows for discussion of wave propagation, transmission, absorption, trapping of orographic gravity waves in weak winds, estimation of wave speeds and periods, and offers an explanation of PSC orientation. This is followed by a brief discussion of geostrophic adjustment, which generates IGW in the process of Rossby wave breaking. The last section summarizes mete-

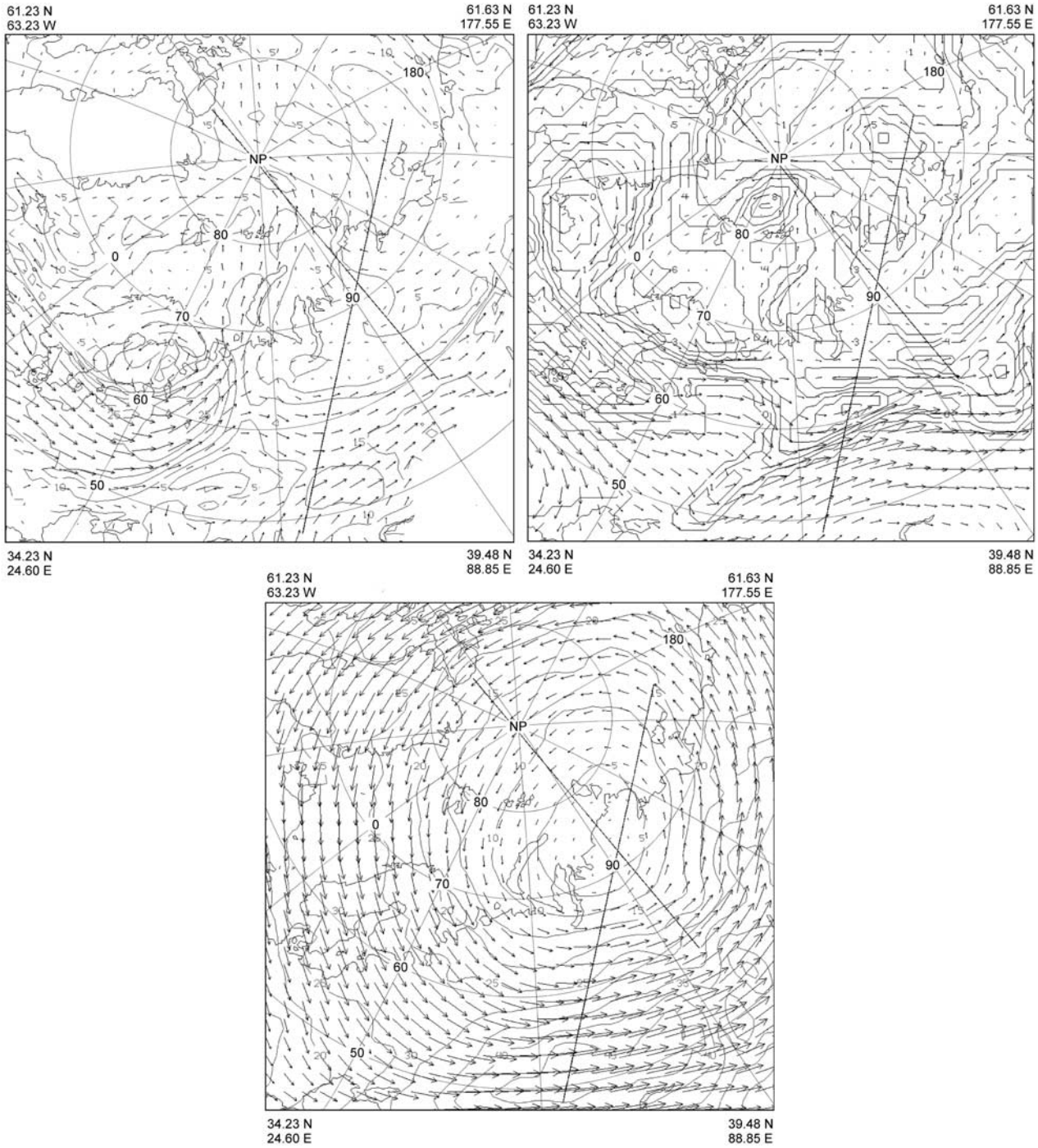


**Figure 14.** UWNMS wind vectors at (a) 1 km, (b) 9 km, and (c) 20 km altitude, at 1300 UT, 7 December 1999. In Figure 14a no vectors are shown where topography exceeds 1 km. Wind speed, contour interval 5 m/s, is shown in Figures 14a and 14c. PV near the tropopause is shown in Figure 14b, contour interval 1 PVU.

orological considerations which may be relevant to theories of PSC microphysics.

### 6.1. Linear Inertia Gravity Wave Theory

[36] Let the $x$ direction be oriented along the polar front jet. Linearizing the primitive equations on an $f$-plane, and assuming vertical wavelengths less than ~80 km, the Boussinesq dispersion relation is obtained:

$$(\omega - \overline{u}k)^2 = f^2 + \frac{N^2(k^2 + l^2)}{m^2}, \tag{1}$$

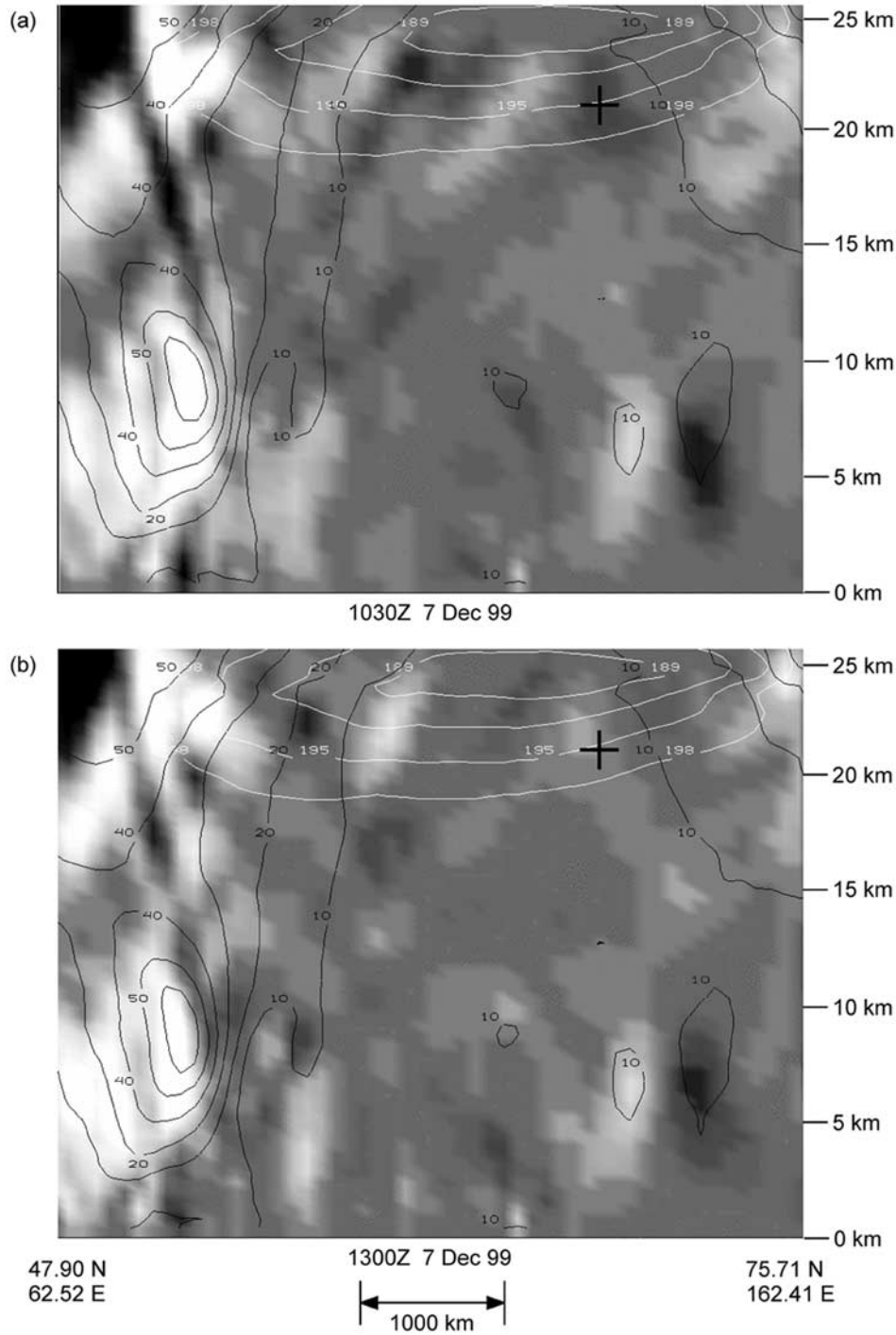


**Figure 15.** Cross sections of UWNMS zonal wind speed (solid contours, 5 m/s interval), vertical motion (gray shading), and temperatures below 198 K (white lines, contour interval 3 K) at (a) 1030 UT and (b) 1300 UT, 7 December 1999, along the southwest-northeast line in Figure 9. The crosshairs are located at 80.6°N, 89.1°E, 21 km, just south of the PSC.

where $\omega$ is a constant wave frequency with respect to the ground, $\overline{u}$ is the horizontal basic state wind (which can vary in the plane perpendicular to the jet), $k$ is the (constant) wave number in the $x$ direction, $l$ is the horizontal wave number in the plane perpendicular to the jet, $m$ is vertical wave number (which varies with $\overline{u}$ and can be positive or negative), $N$ is the buoyancy frequency, and $f$ is the Coriolis parameter [e.g., *Andrews et al.*, 1987]. For wave periods much less than 12 hours one can neglect $f$ in evaluating order of magnitude scale relationships and orientation. For a period of 8 hours this assumption causes an order 20% error in frequency. The upward poleward tilt of the wave phase surfaces in the UWNMS, which indicates upward-poleward wave activity propagation, can be studied by taking the negative root of

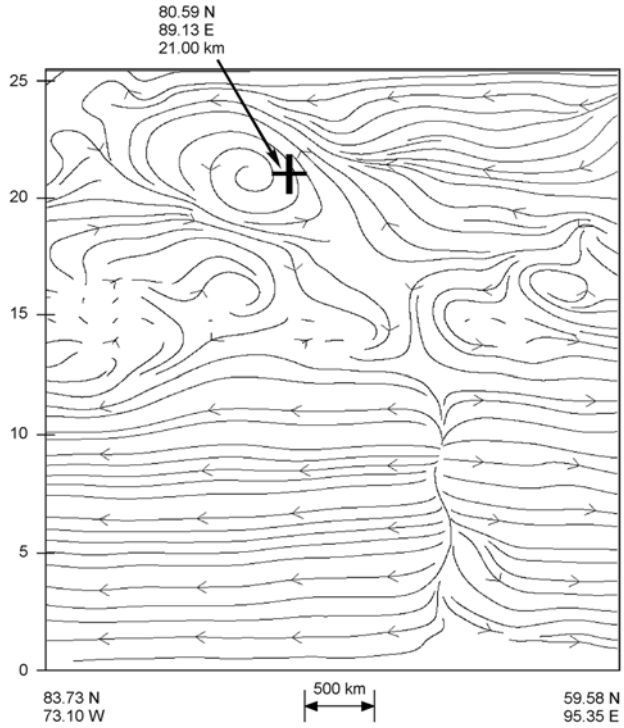


**Figure 16.** Cross section of UWNMS stream function in the plane tangent to the northbound flight path west of Severnaya Zemlya at 1100 UT, 7 December 1999. The crosshairs are located where the observed "PSC2" was encountered a few hours later.

equation (1) with $m < 0$: $\omega = \overline{u}k - \frac{N\left(k^2+l^2\right)^{1/2}}{m}$. Considering the highly elongated horizontal aspect ratio of jet structures one may assume that $k^2 < l^2$, so that

$$\omega \approx \overline{u}k - \frac{Nl}{m} \tag{2}$$

and the cross-jet and vertical group speeds become

$$\left(G_y, G_z\right) \approx \left(\frac{-N}{m}, \frac{Nl}{m^2}\right). \tag{3}$$

The along-jet modal component of the trace velocity, or wave celerity, is $c_x = u_o$, the speed of the flow at the forcing level. Cross-jet and vertical components are $c_y = G_y$ and $c_z = -G_z$. For $m < 0$ the group velocity is upward and poleward along wave crest and trough axes, while individual waves propagate poleward and downward. This is compatible with the orientation of aerosol features on both 7 and 12 December.

[37] A spectrum of waves may be excited by a rapidly evolving jet. A critical surface is encountered wherever $c_x \approx u_o$, where $m \to \infty$ and $G_z \to 0$ (see equations (2) and (3)). As the wave activity ascends in wind shear, waves propagating in the same direction as the wind will tend to get absorbed approaching a critical surface. Waves propagating in the opposite direction will not meet a critical surface, will have a faster group velocity (equation (3)) and a taller vertical-scale (equation (2)). These transmitted IGW traveling antiparallel to the flow will dominate the gravity wave field [*Dunkerton and Butchart*, 1986]. In the case of 12 December the IGW packet was emitted perpendicular to the northward polar front jet (Figures 5 and 6b), but above and poleward of this jet westerlies prevailed (Figure 6c), effectively selecting for southwestward and downward propagating gravity waves near the aerosol thickenings. In the 7 December case the wave field was emitted upward and into the cold pool from the polar front jet folding over western Russia (Figure 14b), encountering weak winds along the path to the PSC (Figures 14b and 14c), experiencing comparatively less filtering by this mechanism. When the wave field reached the coldest part of the vortex near Severnaya Zemlya an upwelling event lasting a few hours that morning probably led to the creation of the isolated, striking PSC.

[38] In the case of orographic waves, $\omega \sim 0$, so that $m \to \infty$ as $\overline{u} \to 0$ at some level above the orography. This suggests that, even if the light surface winds and modest underlying topography near the 7 and 12 December PSCs could generate topographic gravity waves, they would tend to be absorbed in the very slow flow of the lower stratosphere, well below the observed PSCs. Classical conditions for generation of PSCs over orography include very strong surface winds, sufficient to induce resonance. Other distinguishing aspects include substantial orography oriented perpendicular to the flow and PSC occurrence over or close to orography. All of these factors suggest that the aerosol features on 7 and 12 December were most likely not due to orography, but were generated in association with IGW fields propagating away from the polar front jet into the cold pool.

[39] Introducing the wave period, $\tau$, and wavelengths $L_y$ and $L_z$, in the cold pool where $\overline{u}$ is small, equations (2) and (3) become the scale relations

$$\tau \sim \frac{2\pi\, L_y}{N\, L_z}, \tag{2'}$$

$$\left(G_y, G_z\right) \sim \left(\frac{N\, L_z}{2\pi}, \frac{N\, L_z^2}{2\pi\, Ly}\right). \tag{3'}$$

From (2′), assuming $L_z \sim 10$ km, and $N = 0.02$ s$^{-1}$, horizontal wavelengths of ~300 km for 12 December and ~1000 km for 7 December would imply wave periods of ~2.5 and 9 hours, in reasonable agreement with the observations and simulations. From (2′) or (3′), $G_y = c_y \sim 30$ m/s, and $G_z \sim 1$ km/hour for both the northeastward traveling packet on 7 December and the southwestward traveling packet on 12 December.

[40] In an IGW the maximum in upward motion is followed 1/4 cycle later by a minimum in temperature. Once PSC particles are formed they can persist at higher temperatures, hence a PSC can outlast an updraft or a temperature minimum. The pattern of vertical motion along an IGW wave crest is related to the PSC shape, being significantly steeper than the slope of air parcel motions through the PSC. The aspect ratio $L_z/L_y \sim 1/100$ is in agreement with lidar observations of the PSC aspect ratio. This slope is also the angle of energy propagation poleward and upward: $\frac{G_z}{G_y} \sim \frac{L_z}{L_y}$. This relation shows that, for a given $L_y$, shorter waves will be seen at lower altitudes, while taller waves will be seen at higher altitudes, perhaps contributing

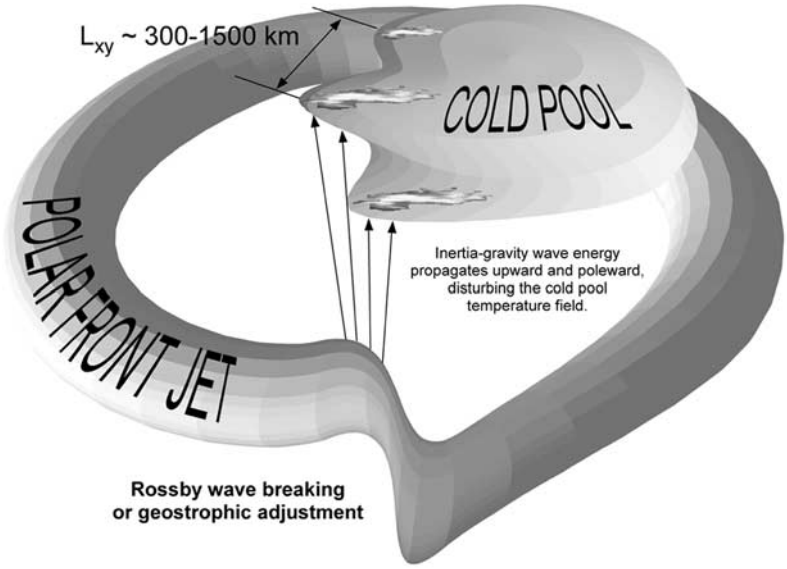


**Figure 17.** Relationship among the polar front jet, synoptic wave breaking, inertia gravity wave radiation into the cold pool, and PSC formation.

to the "banana-shaped" aerosol enhancement features on 12 December.

### 6.2. Rossby Wave Breaking as a Source of IGW

[41] *Rossby* [1938] considered the process by which a fluid on a rotating sphere adjusts to equilibrium. Employing conservation of potential vorticity, he showed that adjustment occurs rapidly, on the order of a rotation period, and that the equilibrium state achieved, a geostrophic jet, is not a rest state. A jet which is changing its shape or speed can only do so through adjusting the relationship between the mass and velocity fields, which occurs through radiation of gravity waves away from the jet [*Gill*, 1982]. A developing baroclinic disturbance is associated with a rapidly evolving upper tropospheric jet. Although the term Rossby wave breaking was first used to describe stratospheric planetary wave behavior [*McIntyre and Palmer*, 1983], the occlusion process may also be described as Rossby wave breaking, where material contours are stretched, folded, and irreversibly deformed. In the process there is a rapid adjustment of the large-scale, rotational flow structure via excitation of divergent modes and their propagation away. This historical model underpins our deduction that many PSCs originate from IGW radiation into the cold pool from preferred locations on the polar front jet where Rossby wave breaking occurs.

[42] A summary of this process is shown in Figure 17. The trajectory of IGW activity has a slope of ~1:100. From equation 3′, energy travels toward the cold pool at ~100 km/hour and upward at ~1 km/hour. In one half day energy could propagate 1000–2000 km into the cold pool and 1–2 scale heights upward. During this time wave absorption processes would significantly reduce wave amplitudes, as suggested by the pattern of temperature perturbations in Figure 9. Thus, IGW generation of PSCs requires that the source be close enough to the cold pool. Since there is usually more than one location around the polar front jet experiencing Rossby wave breaking, a qualitative picture emerges of multiple gravity wave packets "sloshing" the cold pool. In some cases gravity wave packets may constructively interfere, producing PSCs with unusual shapes. This presents an interesting challenge for diagnosis. It also highlights the difficulty in accurately simulating this phenomenon.

### 6.3. Meteorological Aspects of PSC Formation

[43] During the December SOLVE campaign temperatures were often colder than 195 K over a large area and colder than 192 K at some altitudes. Denitrification and dehydration had not yet occurred. Yet PSCs in the cold pool were uncommon. In a dynamically quiescent cold pool, radiative cooling of 0.5–1 K/day leads to both subsidence and lower temperatures. If uniform cooling were all that is required, uniform aerosol enhancements would be observed. Instead, in December PSCs were found in discrete, widely dispersed locations. We hypothesize that local, dynamically induced upward motion is a necessary condition for the formation of a PSC. Once formed, the PSC may last through substantial positive temperature excursions: an aerosol microphysical hysteresis effect [e.g., *Peter*, 1997]. In this scenario, if temperatures are close to the condensation point in the synoptic-scale cold pool, a local reduction of as little as 0.4 K could induce PSC formation. This mechanism would also work for IGW propagating energy downward from the stratospheric polar night jet.

[44] The time tendency of temperature may be important to the microphysics of condensation. IGW can induce local minor temperature changes on the timescale of a few hours. As an IGW axis of upward motion propagates through the stratosphere, the PSC can expand with the wave, so that the edge appears to migrate. The PSC of 7 December is distinct from an orographic PSC in that the feature appears to have propagated relative to quiescent flow. PSCs generated by this mechanism can be found geographically distant from the energy source. Condensation patterns can exhibit a long, uniform wave train or be isolated and extensive. Residence times in IGW PSCs may be considerably longer than in

orographic PSCs. It is interesting to note that the range in pressure and temperature within the PSC on 7 December was 52-26 hPa and 190–198 K, as diagnosed in the UWNMS. The pressure varied by a factor of 2 and the temperature was 8 K warmer at the bottom than at the top of this PSC. These meteorological factors should be considered in microphysical theories of PSC formation.

[45] **Acknowledgments.** We would like to thank the SOLVE science team for their contributions which make this work possible. We thank Duncan Fairlie, Lynn Harvey, Eric Jensen, and Brad Pierce for beneficial conversations and the reviewers for their useful comments. We gratefully acknowledge support from NASA SAGE II Science Team grant NAG-1-2162 and NASA grant NAG5-11303.

## References

Andrews, D. G., J. R. Holton, and C. B. Leovy, *Middle Atmosphere Dynamics*, 489 pp., Academic, San Diego, Calif., 1987.

Avissar, R., E. Eloranta, K. Gurer, and G. J. Tripoli, An evaluation of the large eddy simulation option of the Regional Atmospheric Modeling System in simulating the convective boundary layer: A Fife case study, *J. Atmos. Sci.*, *55*, 1109–1130, 1998.

Browell, E. V., S. Ismail, and W. B. Grant, Differential absorption lidar (DIAL) measurements from air and space, *Appl. Phys. B*, *67*, 399–410, 1998.

Buker, M. L., Nonhydrostatic modeling of gravity waves and tracer transport in the tropical lower stratosphere: First results, thesis, M.S., 95 pp., Univ. of Wis., Madison, 1997.

Burris, J., et al., Lidar temperature measurements during the TOTE/VOTE mission, *J. Geophys. Res.*, *103*, 3505–3510, 1998.

Cariolle, D., S. Muller, F. Cayla, and M. P. McCormick, Mountain waves, polar stratospheric clouds, and the ozone depletion over Antarctica, *J. Geophys. Res.*, *94*, 11,233–11,240, 1989.

Carslaw, K. S., et al., Particle microphysics and chemistry in remotely observed mountain polar stratospheric clouds, *J. Geophys. Res.*, *103*, 5785–5796, 1998a.

Carslaw, K. S., et al., Increased stratospheric ozone depletion due to mountain-induced atmospheric waves, *Nature*, *391*, 675–678, 1998b.

Coy, L., and M. H. Hitchman, Kelvin wave packets and flow acceleration: A comparison of modeling and observations, *J. Atmos. Sci.*, *41*, 1875–1880, 1985.

Dörnbrack, A., M. Leutbecher, R. Kivi, and E. Kyrö, Mountain wave induced record low stratospheric temperatures above northern Scandinavia, *Tellus, Ser. A*, *51*, 951–963, 1998.

Dunkerton, T. J., and N. Butchart, Propagation and selective transmission of internal gravity waves in a sudden warming, *J. Amos. Sci.*, *41*, 1443–1460, 1986.

Gill, A. E., *Atmosphere-Ocean Dynamics*, 662 pp., Academic, San Diego, Calif., 1982.

Grant, W. B., et al., Correlative stratospheric ozone measurements with the airborne UV DIAL system during TOTE/VOTE, *Geophys. Res. Lett.*, *25*, 623–626, 1998.

Gross, M. R., T. J. McGee, R. A. Ferrare, U. Singh, and P. Kimvilikani, Temperature measurements made with a combined Rayleigh-Mie/Raman lidar, *Appl. Optics*, *24*, 5987–5995, 1997.

Hibbard, W. L., and D. Santek, The VIS-5D system for easy interactive visualization, in *Proceedings of Visualization '90*, pp. 28–35, IEEE Press, Piscataway, N. J., 1989.

Hitchman, M. H., M. L. Buker, and G. J. Tripoli, Influence of synoptic waves on column ozone during Arctic summer 1997, *J. Geophys. Res.*, *104*, 26,547–26,563, 1999.

Jascourt, S., Convective organizing and upscale development processes explored through idealized numerical experiments, Ph.D. dissertation, 267 pp., Univ. of Wis., Madison, 1997.

Leutbecher, M., and H. Volkert, Stratospheric temperature anomalies and mountain waves: A three-dimensional simulation using a multi-scale weather prediction model, *Geophys. Res. Lett.*, *23*, 3329–3332, 1996.

McIntyre, M. E., and T. N. Palmer, Breaking planetary waves in the stratosphere, *Nature*, *305*, 593–600, 1983.

Mecikalski, J. R., and G. J. Tripoli, Inertial available kinetic energy and the dynamics of tropical plume formation, *Mon. Weather Rev.*, *126*, 2200–2216, 1997.

Meilinger, S. K., et al., Size-dependent stratospheric droplet composition in lee wave temperature fluctuations and their potential role in PSC freezing, *Geophys. Res. Lett.*, *22*, 3031–3034, 1995.

O'Sullivan, D., and T. J. Dunkerton, Generation of inertia-gravity waves in a simulated life cycle of baroclinic instability, *J. Atmos. Sci.*, *52*, 3695–3715, 1995.

Palmén, E., and C. W. Newton, *Atmospheric Circulation Systems*, 603 pp., Academic, San Diego, Calif., 1969.

Peter, T., Microphysics and heterogeneous chemistry of polar stratospheric clouds, *Annu. Rev. Phys. Chem.*, *48*, 785–822, 1997.

Pfenninger, M., A. Z. Liu, G. C. Papen, and C. S. Gardner, Gravity wave characteristics in the lower atmosphere at South Pole, *J. Geophys. Res.*, *104*, 5963–5984, 1999.

Pokrandt, P. J., G. J. Tripoli, and D. D. Houghton, Processes leading to the formation of mesoscale waves in the midwest cyclone of 15 December 1987, *Mon. Weather Rev.*, *124*, 2726–2752, 1996.

Rossby, C. G., On the mutual adjustment of pressure and velocity distributions in certain simple current systems, *J. Mar. Res.*, *2*, 239–263, 1938.

Sato, K., T. Kumakura, and M. Takahashi, Gravity waves appearing in a high resolution GCM simulation, *J. Atmos. Sci.*, *56*, 1005–1018, 1999.

Tripoli, G. J., An explicit three-dimensional nonhydrostatic numerical simulation of a tropical cyclone, *Meteorol. Atmos. Phys.*, *49*, 229–254, 1992a.

Tripoli, G. J., A nonhydrostatic numerical model designed to simulate scale interaction, *Mon. Weather Rev.*, *120*, 1342–1359, 1992b.

Volkert, H., and D. Intes, Orographically forced stratospheric waves over northern Scandinavia, *Geophys. Res. Lett.*, *19*, 1205–1208, 1992.

Whiteway, J. A., and T. J. Duck, Evidence for critical level filtering of atmospheric gravity waves, *Geophys. Res. Lett.*, *23*, 145–148, 1996.

Whiteway, J. A., et al., Measurements of gravity wave activity within and around the Arctic stratospheric vortex, *Geophys. Res. Lett.*, *24*, 1387–1390, 1997.

Wirth, M., et al., Model-guided Lagrangian observation and simulation of mountain polar stratospheric clouds, *J. Geophys. Res.*, *104*, 23,971–23,981, 1999.

Yoshiki, M., and K. Sato, A statistical study of gravity waves in the polar regions based on operational radiosonde data, *J. Geophys. Res.*, *105*, 17,995–18,011, 2000.

E. V. Browell and W. B. Grant, NASA Langley Research Center, Hampton, VA 23681, USA. (e.v.browell@larc.nasa.gov; w.b.grant@larc.nasa.gov)

M. L. Buker, M. H. Hitchman, and G. J. Tripoli, Department of Atmospheric and Oceanic Sciences, University of Wisconsin, Madison, 1225 W. Dayton St., Madison, WI 53706, USA. (marcus@aos.wisc.edu; matt@aos.wisc.edu; tripoli@aos.wisc.edu)

J. F. Burris and T. J. McGee, NASA Goddard Space Flight Center, Greenbelt, MD 20771, USA. (john.burris@gsfc.nasa.gov; mcgee@hyperion.gsfc.nasa.gov)